

Radiological and non-radiological leaching assessment of
alkali-activated materials containing ground granulated blast furnace
slag and phosphogypsum

Peer-reviewed author version

GIJBELS, Katrijn; Landsberger, Sheldon; SAMYN, Pieter; Iacobescu, Remus Ion;
Pontikes, Yiannis; SCHREURS, Sonja & SCHROEYERS, Wouter (2019)
Radiological and non-radiological leaching assessment of alkali-activated materials
containing ground granulated blast furnace slag and phosphogypsum. In: Science of
the total environment, 660, p. 1098-1107.

DOI: 10.1016/j.scitotenv.2019.01.089

Handle: <http://hdl.handle.net/1942/28168>

1 **RADIOLOGICAL AND NON-RADIOLOGICAL LEACHING ASSESSMENT OF ALKALI-**
2 **ACTIVATED MATERIALS CONTAINING GROUND GRANULATED BLAST**
3 **FURNACE SLAG AND PHOSPHOGYPSUM**

4

5 Katrijn GIJBELS^{a*}, Sheldon LANDSBERGER^b, Pieter SAMYN^c, Remus Ion IACOBESCU^d, Yiannis

6 PONTIKES^d, Sonja SCHREURS^a, Wouter SCHROEYERS^a

7

8 ^a Hasselt University, CMK, Nuclear Technological Centre, Agoralaan, Gebouw H, 3590 Diepenbeek,

9 Belgium

10 ^b Nuclear Engineering Teaching Lab, University of Texas at Austin, Pickle Research Campus, Austin, TX

11 78712, USA

12 ^c Hasselt University, IMO, Applied and Analytical Chemistry, Agoralaan, Gebouw D, 3590 Diepenbeek,

13 Belgium

14 ^d KU Leuven, Department of Materials Engineering, Kasteelpark Arenberg 44, 3001 Leuven, Belgium

15

16 * Corresponding author: Katrijn GIJBELS, +3211292157 (Tel.), +3211268199 (Fax.)

17

18 katrijn.gijbels@uhasselt.be, s.landsberger@mail.utexas.edu, pieter.samyn@uhasselt.be,

19 remusion.iacobescu@kuleuven.be, yiannis.pontikes@kuleuven.be, sonja.schreurs@uhasselt.be,

20 wouter.schroeyers@uhasselt.be

21

22

23 **Abstract**

24 Alkali-activated materials (AAMs) based on ground granulated blast furnace slag (GGBFS) and
25 phosphogypsum (PG) were investigated in order to quantify leaching of naturally occurring
26 radionuclides (NOR) and inorganic non-radiological elements according to an up-flow percolation
27 column test as described in CEN/TS 16637-3. Gamma spectroscopy and neutron activation analysis
28 (NAA) were applied for radiological characterization, inductively coupled plasma optical emission
29 spectrometry (ICP-OES) and ion-chromatography (IC) for chemical characterization. Upon leaching,
30 ^{238}U , ^{226}Ra , ^{210}Pb , and ^{228}Ra were retained very well. Both for ^{232}Th and ^{40}K , a decrease in activity
31 concentration was observed due to leaching and their release was influenced by the use of different
32 alkali activators, which was also the case for the leaching of non-radiological elements. Only a small
33 amount of Al (0.5-0.8%), Ca (0.1-0.2%) and Si (0.1-0.3%) was mobilized, while highest release was
34 observed for K (56-94%), Na (49-88%) and S (71-87%). At first glance, drinking water is not
35 endangered by leaching of NOR following the requirements of the European Drinking Water
36 Directive. From the results for porosity, obtained with mercury intrusion porosimetry (MIP), it was
37 concluded that both the porosity and formation of multiple leachable and non-leachable complexes
38 are determining factors for the release of elements from AAMs.

39

40 **Keywords**

41 Alkali-activated material, ground granulated blast furnace slag, phosphogypsum, naturally occurring
42 radionuclides, leaching

43

44 **1. Introduction**

45 From a sustainability perspective, the reuse of industrial by-products or residues in the production of
46 construction materials has become an indispensable practice to reduce waste production, CO₂

47 emissions, energy and natural resources usage by replacement of primary raw materials. In this
48 respect, Ordinary Portland Cement (OPC) can be replaced by alkali-activated materials (AAMs), which
49 are considered as promising alternative binders due to (1) their excellent performance
50 characteristics, and (2) because they can be synthesized from by-products or residues (Provis, 2017).
51 However, by-products or residues can be characterized by enhanced concentrations of hazardous
52 compounds, such as heavy metals and/or naturally occurring radionuclides (NOR) (Nuccetelli et al.,
53 2015). Therefore, AAMs must be capable to immobilize these particular compounds, starting from
54 the use scenario as well as during demolition, recycling and disposal (end-of-life). Hence in the
55 evaluation of AAMs, the whole life-cycle must be considered.

56 This study describes the incorporation of phosphogypsum (PG) in AAMs based on ground granulated
57 blast furnace slag (GGBFS). PG originates from the phosphate industry, where phosphoric acid is
58 separated from phosphate ore by treatment with sulphuric acid. PG is characterized by enhanced
59 levels of NOR, mainly from the ^{238}U series, provoking many restrictions on its use. Besides, impurities
60 such as P_2O_5 , F^- , organic substances and alkali metals can be incorporated (Tayibi et al., 2009; Wang
61 et al., 2018). PG is disposed of in large stockpiles, occupying vast areas of land which is very costly
62 due to mandatory environmental monitoring and long-term maintenance (Central Pollution Control
63 Board, 2012; Tayibi et al., 2009). Up to 2006, the total amount of PG produced worldwide is
64 estimated to have been about 6 billion tons (International Atomic Energy Agency (IAEA), 2013),
65 consequently large-scale valorization options are needed to consume these vast amounts (Rashad,
66 2017). GGBFS has already been extensively studied for the production of AAMs, being an excellent
67 precursor for alkali activation and allowing the incorporation of precursors which are less suitable,
68 such as PG (Kuo et al., 2014; Lancellotti et al., 2018; Ulubeyli and Artir, 2015). PG participates as an
69 additional source of sulphate, giving rise to additional reaction products compared to AAMs solely
70 based on slags (Nguyen et al., 2018). The levels of NOR in GGBFS are low, consisting of radionuclides
71 from both the ^{238}U and ^{232}Th series (Sas et al., 2017).

72 Concerning NOR in building materials, the European Basis Safety Standards (EU-BSS) Directive
73 (Council Directive 2013/59/Euratom) sets down a framework for screening of gamma exposure from
74 building materials. In addition to outdoor external exposure, the reference level for indoor external
75 exposure emitted by building materials is set at 1 mSv/y (Council of the European Union, 2014). This
76 aspect has been described in detail in a complementary study (Gijbels et al., 2018). Nonetheless, less
77 attention has been paid to the leaching behavior of NOR from building materials (Croymans et al.,
78 2017; Michalik et al., 2018; Mossini et al., 2015). Consequently, there is poor understanding of the
79 potential migration of NOR, especially in the alkaline range of pH, which is the main condition
80 imposed by AAMs. Notwithstanding, reuse of naturally occurring radioactive materials (NORM), such
81 as PG, in building materials may lead to leaching of NOR to groundwater and can consequently affect
82 the quality of drinking water supplies, which could be a concern from the radiation protection point
83 of view (Contreras et al., 2014, 2013). AAMs are often used for stabilization/solidification purposes
84 (Huang et al., 2017; Shi and Fernández-Jiménez, 2006) and consequently low leaching rates are
85 expected. A detailed investigation of NOR leaching is lacking and is presented in this study, aiming to
86 prevent anthropogenic influence on the environment, in particular the contamination of water.
87 Leaching of non-radiological elements (e.g. calcium or sodium) can possess synergistic effects on
88 NOR leaching and should be studied in parallel.

89 Leaching of inorganic constituents from building materials can be assessed either by batch or column
90 leaching tests (Hjelmar et al., 2012; Nebel and Spanka, 2013). Batch tests may underestimate the
91 actual release of contaminants, while column tests provide more reliable field-correlated information
92 (Cappuyens and Swennen, 2008). Moreover, the release behavior during the end-of-life phases of the
93 building material is more accurately predicted when compared to batch tests.

94 The radioactivity of the ^{238}U and ^{232}Th isotope decay chains in processed industrial by-products or
95 residues, such as GGBFS and PG, are mostly characterized to be in disequilibrium resulting in
96 differences in the activity concentration for the radionuclides of a given decay chain (Michalik et al.,

97 2018). For this reason, assessment of leaching requires careful evaluation. Only NOR with a half-life
98 long enough to behave independently in the environment will be considered in the leaching
99 assessment (Michalik et al., 2018).

100 The overall goal of the present study is to assess the leaching of NOR (more specific the long-lived
101 radionuclides from these natural decay chains, and ^{40}K) and non-radiological elements from AAMs
102 based on GGBFS when PG is incorporated. In a conservative approach, the requirements set by the
103 European Drinking Water Directive are used for the evaluation of NOR leaching from AAMs (Council
104 of the European Union, 2013). Also the influence of alkaline solution on leaching and porosity is
105 assessed. In a complementary study, the maximum amount of PG which can be incorporated
106 following the EU-BSS requirements, was determined (Gijbels et al., 2018).

107

108 **2. Experimental**

109 **2.1 Materials**

110 A combination of GGBFS and PG was used as precursor. GGBFS was provided by a Belgian steel
111 company. It was dried in a laboratory oven at 110 °C and subsequently milled to a Blaine fineness of
112 $4050 \pm 200 \text{ cm}^2/\text{g}$, determined according to EN 196-6 (Bureau voor Normalisatie (NBN), 2010). The
113 density of GGBFS was found to be 2.9 g/cm^3 (Quantachrome Multipycnometer MVP-6DC) according
114 to ASTM C204 (ASTM International, 2017). The chemical composition of GGBFS, determined by X-ray
115 fluorescence analysis (Philips, PW 1830), was (in wt%): $36.2 \pm 0.2 \text{ SiO}_2$, $40.3 \pm 0.5 \text{ CaO}$, 11.4 ± 0.2
116 Al_2O_3 , $8.2 \pm 0.1 \text{ MgO}$, $1.1 \pm 0.1 \text{ S}$, $0.8 \pm 0.1 \text{ TiO}_2$, $0.8 \pm 0.1 \text{ Na}_2\text{O}$, $0.5 \pm 0.1 \text{ K}_2\text{O}$ and $0.3 \pm 0.1 \text{ FeO}$. PG
117 was derived from the International Atomic Energy Agency (IAEA) (reference material 434)
118 (Shakhashiro et al., 2011) and was used as received with particle size ranging from 0.5 μm to 30 μm .
119 The matrix composition of PG was provided by the supplier and consisted of (in wt%): 96
120 $\text{CaSO}_4 \cdot 2\text{H}_2\text{O}$, 1-2 P_2O_5 , 1.2 F, 1 SiO_2 and 0.2 Al_2O_3 . The sodium silicate solution used in the
121 experiments was supplied by ABCR GmbH (molar ratio $\text{SiO}_2/\text{Na}_2\text{O} = 3.3$ and 65% water). Sodium

122 hydroxide pellets (99% purity) were purchased from Chem-Lab. Distilled water (ASTM type II) was
123 used throughout the experiments.

124

125 2.2 Sample synthesis

126 Sodium silicate solution was mixed with sodium hydroxide pellets and distilled water to form an
127 alkaline solution with three different molar ratios ($\text{SiO}_2/\text{Na}_2\text{O}=0.75$ and $\text{H}_2\text{O}/\text{Na}_2\text{O}=20$, $\text{SiO}_2/\text{Na}_2\text{O}=0$
128 and $\text{H}_2\text{O}/\text{Na}_2\text{O}=27.8$, $\text{SiO}_2/\text{Na}_2\text{O}=0$ and $\text{H}_2\text{O}/\text{Na}_2\text{O}=18.5$). The alkaline solutions were then left
129 overnight to cool to ambient temperature.

130 Samples were prepared with a GGBFS/PG mass ratio of 9/1 and the mass ratio between the alkaline
131 solution and dry mix (GGBFS + PG) was 3/5. GGBFS and PG were mixed thoroughly until a uniform
132 blend was produced. The alkaline solution was then stirred for 3 min with the dry mix to form a
133 homogeneous paste. The pastes were cast in polymer coated steel molds (20 mm x 20 mm x 80 mm)
134 and allowed to consolidate for 24 h at room temperature having the molds wrapped with plastic foil
135 to avoid water evaporation. After 24 h, the samples were demolded and were stored in sealed
136 storage vessels for further curing at room temperature till they were 28 days old. Table 1 gives an
137 overview of the sample compositions, which were selected for their compressive strength at 28 days
138 (tested in a previous study (Gijbels et al., 2018) and presented in Table 1).

139

Table 1: Composition of the samples

Sample	$\text{SiO}_2/\text{Na}_2\text{O}$	$\text{H}_2\text{O}/\text{Na}_2\text{O}$	wt% GGBFS	wt% PG	Alkaline solution/dry mix	Compressive strength (MPa)
Sample 1	0.75	20.0	90	10	0.6	52.8
Sample 2	0	27.8	90	10	0.6	16.0
Sample 3	0	18.5	90	10	0.6	22.3

140

141 2.3 Leaching test

142 The leaching of non-volatile inorganic NOR and non-radiological elements as a function of liquid-
143 over-solid ratio (L/S) was assessed by means of an up-flow percolation test as described in CEN/TS
144 16637-3 (European Committee for Standardization, 2016). After a curing period of 28 days, samples
145 were dried in a laboratory oven at 40 °C till constant mass, whereafter they were cooled down in a
146 desiccator. Subsequently, samples were crushed till 45% by mass of the test sample had a particle
147 size lower than 4 mm, while 100% by mass had a particle size lower than 16 mm. For the leaching
148 test, 90 g of sample was placed in a column made of glass with an inner diameter of 30 mm and a
149 length of 200 mm. In the top and bottom of the column, a filter paper (Schleicher & Schuell, nr. 595)
150 was fixed, and the outlets were connected with Viton® tubing material with an inner diameter of 1.6
151 mm. A volumetric peristaltic pump (SP100 OEM fixed flow peristaltic pump, APT Instruments)
152 pumped the leachant through the setup with a flow rate of 0.096 ml/min. Distilled water was used as
153 leachant solution to allow a rapid screening of potentially leachable elements and the results are
154 independent of variable local surface, ground- and rainwater chemistry. A saturation period of 20 h
155 was applied whereafter 7 eluate fractions were collected at predefined intervals (0.10 ± 0.02 l/kg,
156 0.10 ± 0.02 l/kg, 0.30 ± 0.05 l/kg, 0.50 ± 0.05 l/kg, 1.00 ± 0.05 l/kg, 3.0 ± 0.1 l/kg, 5.0 ± 0.2 l/kg) until a
157 cumulative L/S of 10.0 ± 0.5 l/kg was reached. The bottles for collection of the eluates were covered
158 with film in order to minimize carbonation. Due to their small volume, the first 2 eluate fractions
159 were diluted by a factor 2. The pH (HI2211 pH/ORP Meter, HANNA Instruments) and conductivity
160 (Konduktometer CG 858, Schott Geräte) of each eluate fraction was measured immediately after
161 collection. Leaching tests were done under laboratory conditions (temperature 20 ± 2 °C, relative
162 humidity about 50%). Between each leaching test, the set-up was first rinsed with diluted (0.1 mol/l)
163 nitric acid (65%, supplied by Merck) and thereafter with distilled water. After leaching, the samples
164 were dried in a laboratory oven at 100 °C till constant mass.

165

166 **2.4 Analysis procedure for naturally occurring radionuclides**

167 For the analysis of NOR, samples were radiometrically counted before (A_0) (in Bq/kg dry mass) and
168 after (A_f) (in Bq/kg dry mass) leaching, and the release is calculated with Eq. 1:

169
$$Release (\%) = \left[\frac{A_0 - A_f}{A_0} \right] \times 100 \text{ (Eq. 1)}$$

170 For the analysis of ^{226}Ra , ^{210}Pb , ^{228}Ra and ^{40}K , samples were gamma spectroscopically counted (A_0)
171 after enclosing radon-tight in a sealed cylindrical polystyrene container of 55 mm diameter and 105
172 mm height for 30 days to reach secular equilibrium of the progenies. Samples were measured on top
173 of a hyper-pure germanium (HPGe) detector (Mirion Technologies (Canberra) model BE5075-7500SI).
174 Shielding against the background radiation was achieved by 0.2 cm copper and 10 cm lead. The
175 system was calibrated with respect to energy using standard sources. The relative efficiency of the
176 detector is 48%, and its energy resolution is 0.346, 0.587 and 1.768 at full width half maximum
177 (FWHM) from 5.9 keV, 122 keV and 1332.5 keV, respectively. The efficiency (ϵ) as a function of the
178 gamma energy (in keV) was determined using Canberra Laboratory Sourceless Calibration software
179 (LabSOCS) by loading the geometry dimensions, mass, shape, material composition and detector
180 configuration and position for each measurement setup. The data and spectra were recorded by a
181 Lynx MCA. The sample measuring time was 67 h. The background spectrum measured under the
182 same conditions with an empty sealed beaker was used to correct the net peak area of measured
183 gamma rays from the samples. The activities were calculated by the software program Genie 2000
184 from Canberra. The activity of ^{226}Ra and progeny was estimated from the full energy peaks of ^{214}Bi
185 (609.3 keV, 1120.3 keV, 1729.6 keV and 1764.5 keV) and ^{214}Pb (351.9 keV). The activity of ^{210}Pb is
186 determined by its 46.5 keV full energy peak. The activity of ^{228}Ra was estimated by the 911.2 keV full
187 energy peak of ^{228}Ac . The ^{40}K activity concentration was estimated using its 1460.8 keV gamma peak.
188 After leaching and drying, samples were enclosed again for 30 days, whereafter they were counted
189 (A_f) again with the same procedure as for A_0 .

190 For the analysis of ^{238}U and ^{232}Th , thermal and epithermal neutron activation analysis (NAA) was
 191 chosen for determination of A_0 and A_f . Before and after leaching, 3 g of the dried sample was
 192 separated, homogenized with a mortar and passed through a 250 micron filter. Thereafter, the
 193 sample was placed in a polyethylene container. ^{238}U was determined using epithermal neutrons with
 194 a neutron flux of $\sim 2.25 \times 10^{12}$ n cm²/s for an irradiation time of 2 min at 500 kW with a decay time of
 195 10 min and a counting time of 5 min. For analysis of ^{232}Th , thermal neutrons were used with a
 196 neutron flux of $\sim 4.5 \times 10^{12}$ n cm²/s and irradiated for 3 h at 950 kW with a decay time of 2 weeks and
 197 a counting time of 4 h. All neutron irradiations were performed using the TRIGA MARK II 1.1 MW
 198 reactor at the Nuclear Engineering Teaching Lab (University of Texas). A description of the
 199 experimental conditions is shown in Table 2. ^{238}U was determined by the 74.5 keV gamma-ray of ^{239}U
 200 ($t_{1/2} = 25$ min) and ^{232}Th by the 311.9 keV gamma-ray of ^{233}Pa ($t_{1/2} = 27.7$ days) with a HPGe ORTEC
 201 detector with a FWHM of 2.1 keV gamma-ray of 1332.4 keV ^{60}Co gamma-ray and efficiency of 32%.
 202 Energy calibration of the detector was performed using ^{152}Eu . Certified uranium and thorium
 203 standards of 10 $\mu\text{g/g}$ were prepared from Inorganic Ventures. Certified reference materials from the
 204 National Institute of Standards and Technology (NIST) were used for quality control measurements.
 205 The NAA values were in excellent agreement with the NIST values as seen in Table 3.

206 **Table 2:** Irradiation and decay information

Nuclide	Technique	Power	Irradiation time	Decay time	Counting time
^{238}U	Epithermal	500 kW	2 min	10 min	5 min
^{232}Th	Thermal	950 kW	3 h	2 weeks	4 h

208 **Table 3:** NAA results as compared to NIST certified values

	NAA results	NIST certified values
1632d coal	1.43 ± 0.05 $\mu\text{g/g}$ (Th)	1.428 ± 0.035 $\mu\text{g/g}$ (Th)

1633c fly ash	23.8 ± 0.8 µg/g (Th)	23.0 ± 0.4 µg/g (Th)
1632d coal	0.502 ± 0.019 µg/g (U)	0.517 ± 0.012 µg/g (U)
2709a soil	3.09 ± 0.11 µg/g (U)	3.15 ± 0.05 µg/g (U)

209

210 The overall uncertainties for the samples and standards were the counting statistics for the uranium
 211 and thorium standards, the uncertainties in the concentrations and counting statistics for the
 212 samples of certified reference materials all taken in quadrature. For all measured NOR, the values for
 213 A_f were corrected for mass loss during leaching. The criteria for release of NOR to groundwater are
 214 specified in the Euratom Drinking Water Directive 2013/51/Euratom (Council of the European Union,
 215 2013).

216

217 2.5 Analysis procedure for non-radiological elements

218 The leaching of non-radiological elements was assessed as a function of L/S (7 eluate fractions) using
 219 an inductively coupled plasma optical emission spectrometer (ICP-OES, Perkin Elmer Optima 8300,
 220 RSD < 2%) for analysis of Al, Ca, Fe, K, Mg, Na, P, Pb, S and Si, and ion-chromatography (IC, Dionex
 221 DX120) for analysis of Cl and F. For IC, an analytical column (IonPac AS14A) with a conductivity
 222 detector was used, and the pH of the eluates was buffered using 1 mM NaHCO₃ (supplied by Merck)
 223 and 8 mM Na₂CO₃ (supplied by Merck). The detection limits (DL) for the quantification of given
 224 elements are shown in Table 4.

225 **Table 4:** DL for ICP-OES (Al, Ca, Fe, K, Mg, Na, P, Pb, S and Si) and IC (Cl and F)

Element	Al	Ca	Fe	K	Mg	Na	P	Pb	S	Si	Cl	F
DL (in mg/l)	< 0.1	< 0.1	< 0.5	< 7	< 0.1	< 1	< 1	< 0.5	< 5	< 0.5	0.1	1

226

227 2.6 Mercury intrusion porosimetry

228 Mercury intrusion porosimetry (MIP) was applied on samples after 28 days of curing. After their
 229 curing period, samples were dried at 40 °C in a laboratory oven till constant mass, whereafter they
 230 were cooled down in a desiccator. MIP was governed by the Washburn-Laplace equation (Cook and
 231 Hover, 1993; Washburn, 1921):

$$232 \quad P = \frac{4\gamma\cos\theta}{d} \quad (\text{Eq.2})$$

233 where P is the mercury injection pressure (Pa), γ is the surface tension of mercury (N/m), θ is the
 234 contact angle between solid and mercury (°), and d is the pore access diameter (m). The tests were
 235 performed with a Micromeritics Autopore IV 9500 V1.07 mercury porosimeter with a maximum
 236 injection pressure of 207 MPa. By assuming a contact angle of 130° and a mercury surface tension of
 237 485×10^{-3} N/m, the minimum pore access diameter reached is about 6×10^{-9} m.

238

239 3. Results and discussion

240 3.1 Leaching of naturally occurring radionuclides

241 The leaching of NOR was assessed by means of gamma spectroscopy (^{226}Ra , ^{210}Pb , ^{228}Ra and ^{40}K) and
 242 NAA (^{238}U and ^{232}Th) by radiometrically counting the samples before (A_0) and after (A_f) leaching with
 243 a cumulative L/S of 10.0 ± 0.5 l/kg. An overview of the results is shown in Table 5.

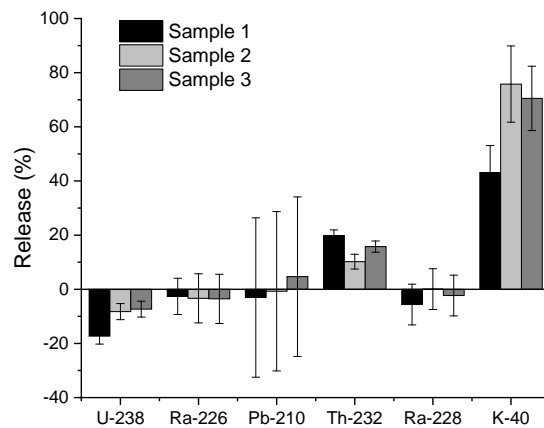
244 **Table 5:** A_0 and A_f (in Bq/kg) for ^{238}U , ^{226}Ra , ^{210}Pb , ^{232}Th , ^{228}Ra and ^{40}K

		^{238}U	^{226}Ra	^{210}Pb	^{232}Th	^{228}Ra	^{40}K
Sample 1	A_0	65.2 ±	125.9 ±	67.0 ±	32.7 ±	30.4 ±	79.8 ±
		0.9	5.7	9.9	0.5	1.1	3.6
	A_f	76.5 ±	129.3 ±	69.0 ±	26.2 ±	32.1 ±	45.4 ±
		1.1	2.8	10.1	0.2	1.2	2.5
Sample 2	A_0	75.8 ±	136.2 ±	68.1 ±	32.6 ±	32.6 ±	88.7 ±

		1.2	6.2	10.1	0.7	1.2	4.0
	A_f	82.0 ±	140.7 ±	68.6 ±	29.3 ±	32.6 ±	21.5 ±
		1.2	6.4	10.1	0.2	1.2	2.1
Sample 3	A_0	72.2 ±	129.2 ±	65.3 ±	33.2 ±	30.9 ±	77.5 ±
		1.1	5.8	9.6	0.5	1.1	3.5
	A_f	77.5 ±	133.7 ±	62.3 ±	27.9 ±	31.6 ±	22.8 ±
		1.1	6.1	9.2	0.2	1.2	1.7

245

246 From Table 5, it can be observed that the activity concentrations for the NOR from the ^{238}U decay
247 chain (i.e. ^{238}U , ^{226}Ra and ^{210}Pb) vary, indicating disequilibrium (as a consequence of the enhanced
248 ^{226}Ra concentration in PG). The ^{232}Th decay chain is assumed to be equilibrium since the activity
249 concentrations of ^{232}Th and ^{228}Ra are equal. In general, the radionuclides from the ^{238}U decay chain
250 show higher activity concentrations compared to the ones from the ^{232}Th decay chain. As a result of
251 the up-flow percolation leaching test, the activity concentrations of ^{226}Ra , ^{210}Pb and ^{228}Ra remained
252 the same (within the boundaries of their uncertainty) for all samples, while the activity
253 concentrations of ^{238}U were slightly higher after leaching. It can be concluded that ^{238}U , ^{226}Ra , ^{210}Pb
254 and ^{228}Ra were retained very well in the solid matrix. For all samples, both for ^{232}Th and ^{40}K , a
255 decrease in activity concentration was observed due to leaching, indicating that these nuclides left
256 the solid matrix. In Fig. 1, the release (in %) of NOR, calculated with Eq. 1, is shown.



257

258

Figure 1: Release of NOR as a consequence of leaching

259 The release of ^{232}Th was highest for sample 1 ($19.9 \pm 2.0\%$), while it was lowest for sample 2 ($10.2 \pm$
 260 2.7%). For sample 3, release of ^{232}Th was $15.8 \pm 2.1\%$. For ^{40}K , the opposite was observed, with the
 261 highest release for samples synthesized with a sodium hydroxide solution ($75.8 \pm 14.1\%$ for sample 2
 262 and $70.5 \pm 11.9\%$ for sample 3), while the use of a sodium silicate solution resulted in lowest ^{40}K
 263 release (i.e. $43.1 \pm 10.0\%$).

264 Although ^{232}Th and ^{238}U are both actinides, ^{238}U was not released upon leaching. There is only limited
 265 published data on the solubility of actinides in cementitious pore waters, which concentrates mostly
 266 on the effect of additives, e.g. EDTA or plasticizers (Colàs et al., 2013; Kitamura et al., 2013).

267 Regarding the binding mechanisms of actinides to cement, less information exists on thorium,
 268 compared to uranium (Evans, 2008). Thorium has a very stable tetravalent oxidation state (Choppin
 269 et al., 2001), while uranium is expected to exist in the form of U^{6+} in an alkaline environment (Evans,
 270 2008). Most likely, thorium forms leachable and non-leachable complexes with other chemical
 271 species upon alkali activation. In aqueous media, thorium is almost always present as Th^{4+} (Rand et
 272 al., 2008) and in alkaline solutions thorium is expected to form thorium hydroxide complexes
 273 ($\text{Th}_m(\text{OH})_{4m}$) (Rand et al., 2008). Also, high pH values give rise to carbonates, resulting in the
 274 formation of mixed thorium-hydroxo-carbonate complexes and thorium carbonate complexes

275 (Altmaier et al., 2005, 2006). Several other chemical species are available for complexation, of which
276 all of them show different thermodynamic properties. There is no evidence for complex formation
277 between Th^{4+} and ClO_4^- , while Th^{4+} forms strong complexes with fluoride (with stoichiometry ThF_n^{4-n} ,
278 with n from 1 to 6) (Rand et al., 2008). The formation of species like $\text{Th}(\text{SO}_4)_n^{4-2n}$ (with n from 1 to 4) is
279 also reasonable because of their very high solubility (Rand et al., 2008). However, the extent to which
280 expected thorium complexes are formed is out of the scope of this research paper. Since thorium
281 leaching was highest for sample 1, the use of a sodium silicate solution gives rise to the formation of
282 more leachable thorium complexes, compared to sodium hydroxide activated samples.

283 Upon alkali activation, the formation of uranium-mineral phases is responsible for its retention in the
284 solid phase. This was already demonstrated in several studies on cementitious materials (Matzen et
285 al., 2000; Sutton et al., 2003), wherein uranium gets adsorbed to silicate surfaces (Sylwester et al.,
286 2000; Tits et al., 2015) and incorporated into the C-S-H (calcium-silicate-hydrate) structure (Felipe-
287 sotelo et al., 2017; Tits et al., 2015), limiting its solubility. Due to the incorporation of PG containing
288 remnants of phosphoric acid, the formation of uranium-phosphate phases may be evident, which
289 were also demonstrated in cement (Wellman et al., 2007). Highest release was observed for
290 potassium, which acts as charge-balancing ion at the negatively charged silicate surface sites (Tänzer
291 et al., 2017). Since potassium belongs to the group of salts, it shows pH independent leaching.
292 Furthermore, as discussed in section 3.2, potassium shows the same leaching behavior as sodium.
293 The release of potassium and sodium is higher for sodium hydroxide activated samples, because their
294 excessiveness was higher compared to sample 1. Radium and lead were retained very well. Since
295 radium is chemically very similar to calcium, a multiphase immobilization is expected, as explained in
296 (Gijbels et al., 2018). The immobilization of lead is due to its precipitation as $\text{Pb}(\text{OH})_2$ in the solid
297 structure (Koplík et al., 2016).

298 The leaching of the different isotopes is affecting the destiny of thorium itself or its daughters to very
299 different degrees. Since the long living isotopes ^{232}Th ($t_{1/2} = 14 \cdot 10^9$ y) and ^{230}Th ($t_{1/2} = 75.4 \cdot 10^3$ y) are

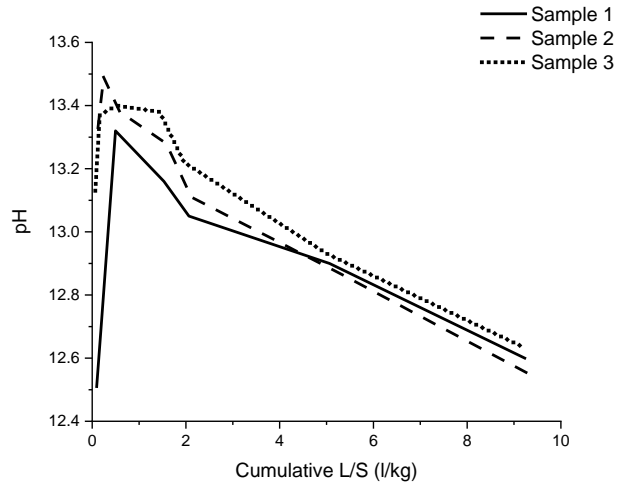
300 chemically the same elements, their leaching behavior is expected to be similar. Leaching of ^{230}Th can
301 have influence on the equilibria in its respective decay chain, and will in the very long term result in
302 enhanced concentrations of ^{226}Ra and progeny in soil and soil water. Since ^{232}Th is the primordial
303 element of its decay chain, its leaching behavior will not give rise to disequilibria, but in the long term
304 lead to slightly lower activity concentrations for all its daughters in the building material.

305 Referring to the European Drinking Water Directive (Council of the European Union, 2013), none of
306 the NOR considered (i.e. ^{238}U , ^{234}U , ^{226}Ra , ^{228}Ra , ^{210}Pb and ^{210}Po) leached out from the solid AAM
307 matrix. At first glance, drinking water is not endangered. However, the ^{226}Ra concentration in soil and
308 soil water is likely to increase as a consequence of ^{230}Th leaching. ^{210}Pb (and consequently ^{210}Po)
309 concentrations are not expected to be of concern because ^{210}Pb was retained in the solid matrix and
310 the half-life of ^{226}Ra is 1600 y. However, the extent to which concentrations will rise or decline,
311 requires advanced modeling, and is also influenced by geochemical and biological processes
312 occurring during the life-time of AAMs. Also, additional alpha- and beta spectroscopy are desirable to
313 confirm the statements about ^{210}Pb and ^{210}Po , respectively.

314

315 **3.2 Leaching of non-radiological elements**

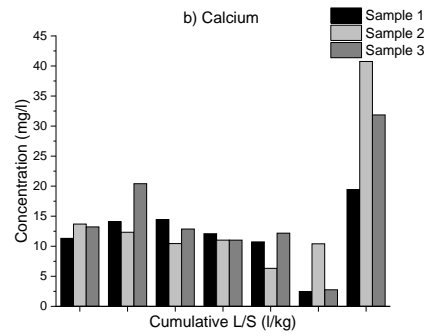
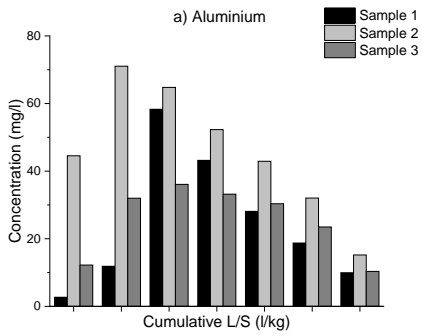
316 The leaching of non-radiological elements was assessed by means of ICP-OES and IC as a function of
317 L/S. For Fe, Mg, P and Pb the concentrations in the eluates were below the detection limits (see
318 Table 4). The change in pH during the column experiments is illustrated in Fig. 2. The general trends
319 in eluate pH were similar for all samples. Initially, the pH increased during the first 2 fractions,
320 followed by a decrease from approximately 13.4 to 12.6. The pH increase is attributed to the
321 dissolution of alkaline elements, such as sodium and potassium, and sulphate (SO_4^{2-}). There is no
322 doubt that the eluate pH will decrease with increasing L/S.



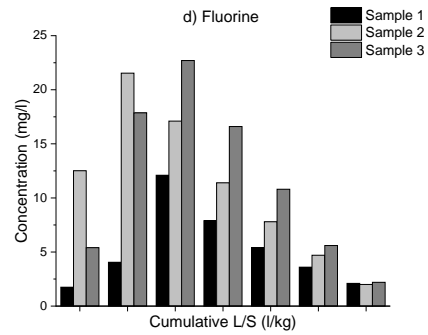
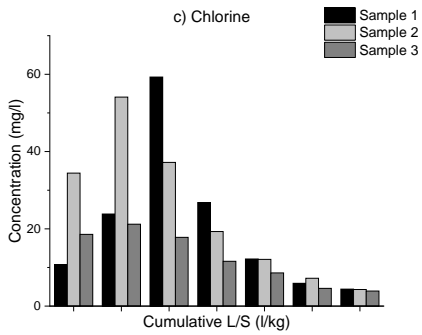
323

324

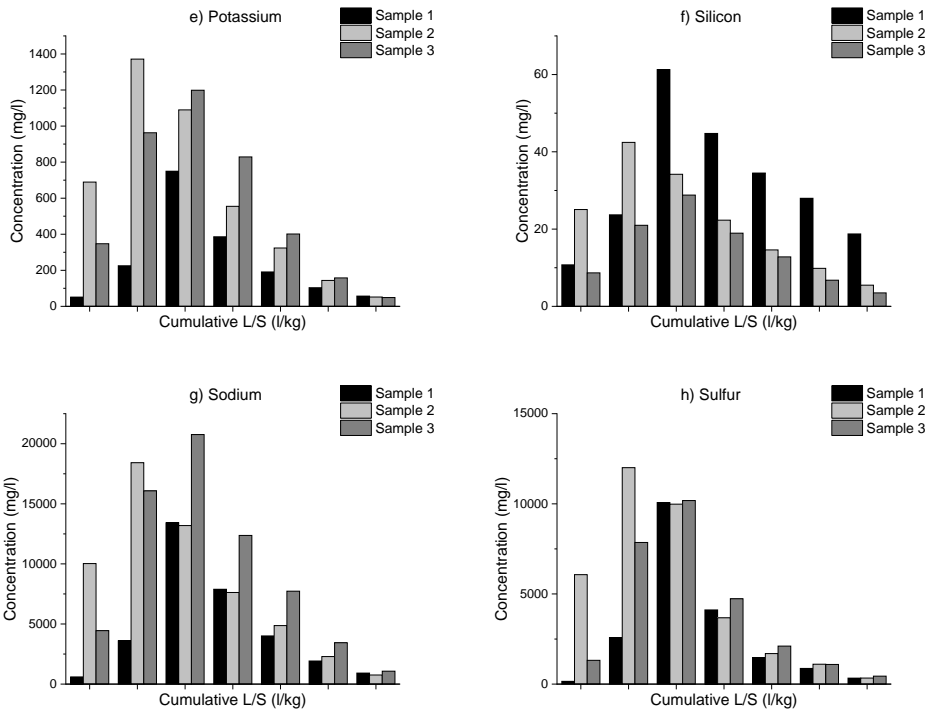
Figure 2: Eluate pH as a function of cumulative L/S



325



326

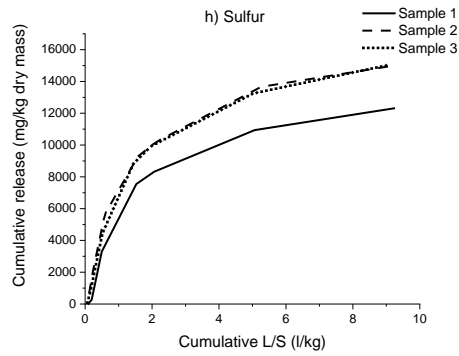
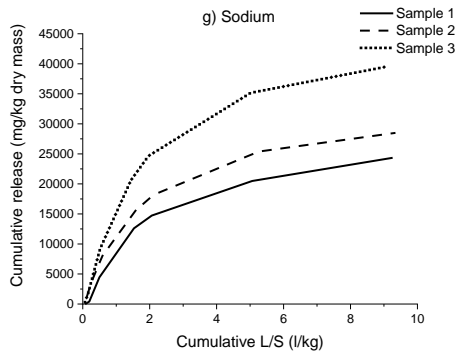
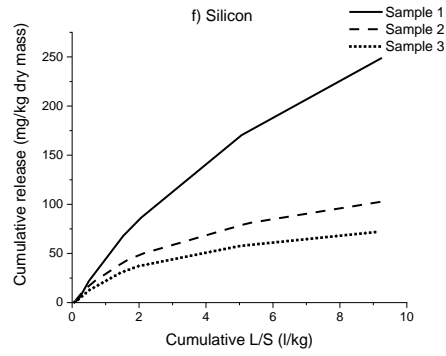
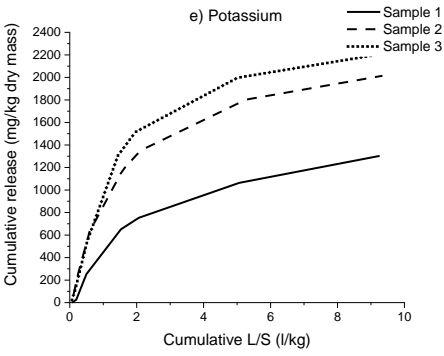
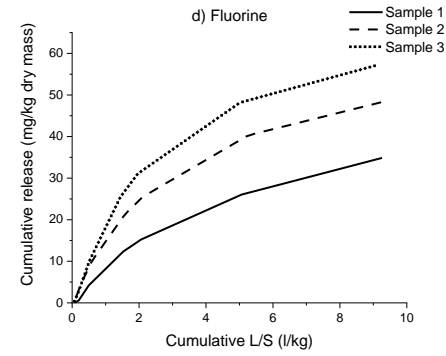
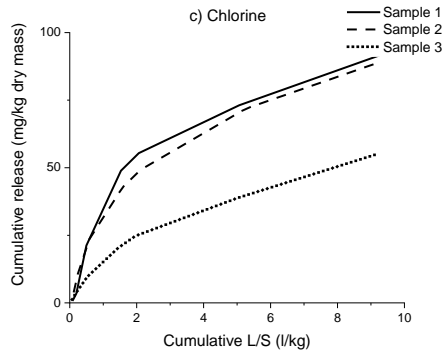
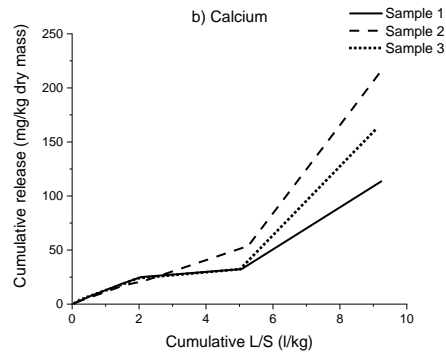
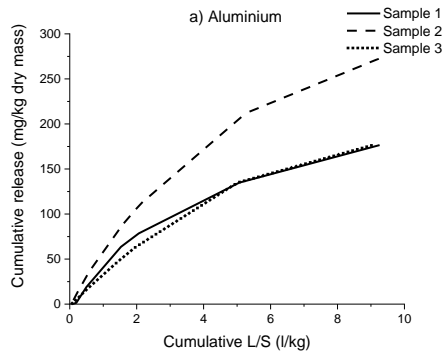


327

328

329 **Figure 3:** Concentration as a function of cumulative L/S for a) aluminium, b) calcium, c) chlorine, d)
 330 fluorine, e) potassium, f) silicon, g) sodium and h) sulfur

331 Fig. 3 reports the concentrations (in mg/l) as a function of cumulative L/S for Al, Ca, Cl, F, K, Si, Na
 332 and S. The release of Fe, Mg, P and Pb is not shown because neither of the eluates contained
 333 measurable concentrations of these elements. Looking at the results reported in Fig. 3, it can be
 334 noticed that the trends of mass release for the different samples are quite similar. This reveals on the
 335 one hand a similar behavior of the samples, and on the other hand, a good reproducibility of the
 336 column test and the consistency of leaching data. The release mechanisms for the measurable
 337 elements were investigated in order to predict the long term release of these during the use scenario
 338 as well as end-of-life phases of the AAM. Ca shows a different release mechanism compared to the
 339 other elements investigated, which also remained unidentified following CEN/TS 16637-3. Al, Cl, F, K,
 340 Si, Na and S show pH dependent solubility controlled release.



341

342

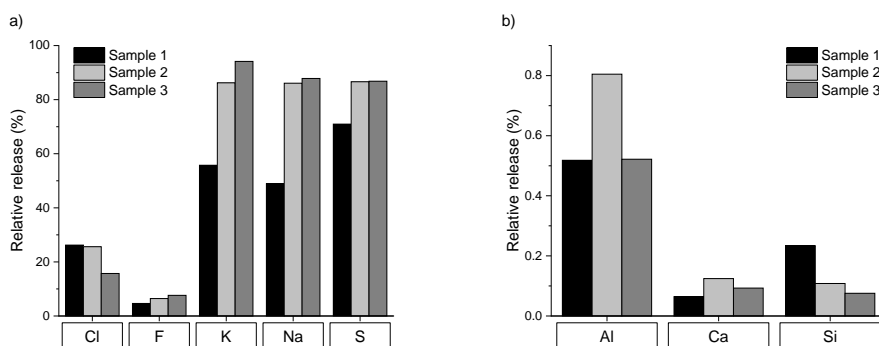
343

344

345 **Figure 4:** Cumulative release as a function of cumulative L/S for a) aluminium, b) calcium, c) chlorine,
 346 d) fluorine, e) potassium, f) silicon, g) sodium and h) sulfur

347 In Fig. 4, the cumulative release (in mg/kg dry mass) as a function of cumulative L/S for Al, Ca, Cl, F, K,
 348 Si, Na and S is depicted. It is clear that the use of different alkali activators substantially affected the

349 leaching capacity of the samples, although the evolution patterns were quite similar. The cumulative
 350 release of Al, Cl, F, K, Si Na and S increased progressively with respect to L/S. A sharp increase of Ca
 351 concentration in the eluates was observed for L/S 10.0 ± 0.5 l/kg. This behavior can be attributed to
 352 the sequential mode of leaching, where initially the depletion of SO_4^{2-} occurs and Ca mobility is
 353 impeded, whereafter Ca transport is facilitated. The use of a sodium silicate solution resulted in
 354 highest cumulative release of Si, while Na and K release were highest in case of sodium hydroxide
 355 solutions, indicating that these elements were in excess. More Al was leached when the H_2O content
 356 in the alkali activator was higher. Cl was immobilized better when a sodium hydroxide solution was
 357 used, while the opposite trend was observed for F for which sample 1 was the best performing
 358 immobilization matrix. The leaching of Cl and Si was higher for sample 1, which showed also the
 359 highest ^{232}Th release. However, it is expected that multiple leachable thorium complexes were
 360 formed, making it impossible to predict to which extent they individually contribute to ^{232}Th leaching
 361 in this case study.



362
 363 **Figure 5:** Relative release for a) chlorine, fluorine, potassium, sodium and b) aluminium, calcium and
 364 silicon

365 By comparing the cumulative release (in mg/kg dry mass) of each element provided by the column
 366 test (at cumulative L/S 10.0 ± 0.5 l/kg) with the total content, the relative release (in %) was
 367 calculated. Results are shown in Fig. 5. Only a small amount of Al, Ca and Si is mobilized, at least if
 368 the environmental conditions (pH, temperature, flow rate) are similar to the tested ones. In fact, the

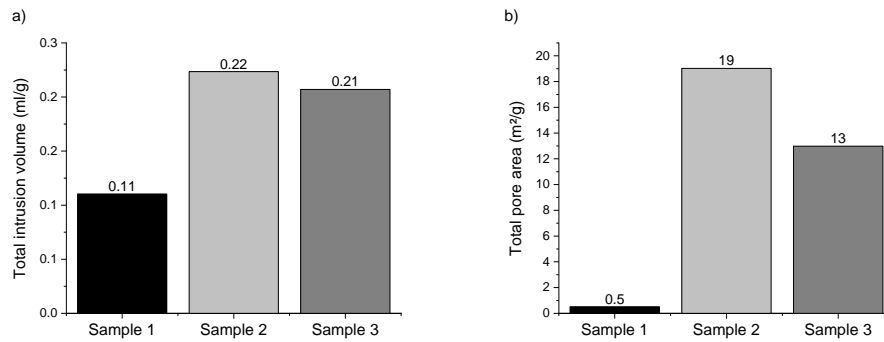
369 release percentage was about 0.5 to 0.8% for Al, 0.1 to 0.2% for Ca and 0.1 to 0.3% for Si. The highest
370 mobility was observed for K, Na and S with release percentages up to 56-94%, 49-88% and 71-87%,
371 respectively. During the hydration process, some K and Na may have been replaced by Ca. Lowest
372 release for K, Na and S was observed for sample 1. Release of Cl was 16-26% and for F was 4-8%.
373 Except for S, the elements originating from PG (i.e. Ca, Cl and F) are fairly well retained in the AAM
374 structure, which is good from the environmental point of view. Since the relative release of Na and S
375 are similar for sample 2 and sample 3, it is expected that the excessive amounts of Na resulted in
376 soluble thenardite formation.

377 In the long term, it is expected that the pH generally will decrease to neutral, and the release of
378 constituents will decline. However, it is worth pointing out that long-term field predictions based on
379 these results should be treated with caution since it neglects different geochemical and biological
380 processes which are likely to occur during the life-time of the AAMs, and that can significantly
381 influence the release. Considering the European Drinking Water Directive (Council of the European
382 Union, 2013), the non-radiological elements of concern in this particular case are Al, Cl, F, Na and S,
383 for which modelling and monitoring is required in case these AAMs are used in the immediate
384 vicinity of a drinking water supply. It is also important to note that the pH of drinking water should be
385 lower than 9.5.

386

387 **3.3 Mercury intrusion porosimetry**

388 The results from MIP are shown in Fig. 6 and Fig. 7. From Fig. 6, it is observed that the final intruded
389 pore volumes for sample 2 and sample 3 are almost double the volume intruded for sample 1. Also
390 the total pore area was much larger for samples activated with sodium hydroxide. The highest
391 H₂O/Na₂O in the alkali activator (i.e. sample 2) led to highest total intrusion volume and total pore
392 area (0.22 ml/g and 19 m²/g, respectively). The data comply with those found by (Nedeljković et al.,
393 2018; Park et al., 2014) on alkali-activated GGBFS.



394

395

Figure 6: a) Total intrusion volume and b) total pore area

396

In Fig. 7 the cumulative pore volume distribution is shown. The pore size distribution of sample 2 and

397

sample 3 are similar, while the curve shape of sample 1 is quite different. Sample 1, activated with a

398

sodium silicate solution, shows a higher amount of pores with diameters in the range of 1 μm to 100

399

μm , compared to the other samples. In the range from 10 nm to 1 μm , there is almost no increase in

400

pore volume for sample 1, resulting in lowest cumulative pore volume. The use of a sodium

401

hydroxide solution increases the cumulative pore volume, with highest amount of pores in the range

402

from 10 nm to 300 nm. A higher $\text{H}_2\text{O}/\text{Na}_2\text{O}$ for a sodium hydroxide solution (i.e. sample 2) gives rise

403

to a lower amount of pores in the range from 100 nm to 100 μm , but a higher amount of pores in the

404

range from 10 nm to 100 nm, compared to sample 3.

405

For most investigated elements (i.e. ^{40}K , Al, Ca, F, K, Na and S), a lower pore volume and pore surface

406

area of the AAM results in lowest release upon leaching, which was the case for sample 1 activated

407

with a sodium silicate solution. On the contrary, the release of ^{232}Th , Cl and Si was higher for sample

408

1. It can be concluded that both the porosity and formation of multiple leachable and non-leachable

409

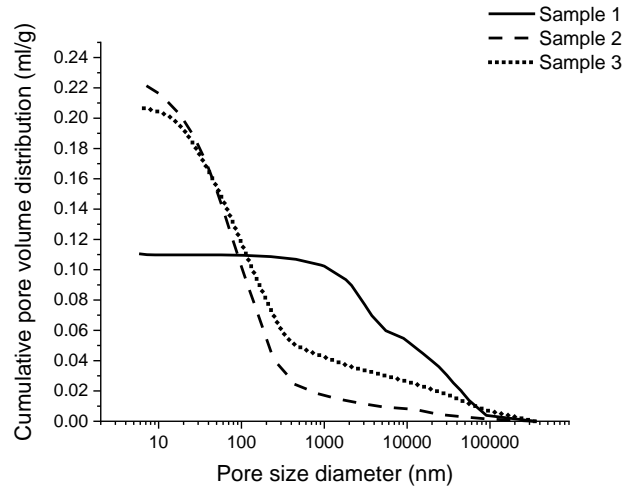
complexes are determining factors for the release of elements from AAMs. Further investigation of

410

the formed complexes upon alkali activation is needed to validate the hypothesis and further

411

investigate the influence of alkali activator.



412

413

Figure 7: Cumulative pore volume distribution

414

415 **4. Conclusions**

416 Leaching of NOR and inorganic non-radiological elements from AAMs based on GGBFS when PG was
 417 incorporated, was assessed. It is concluded that ^{238}U , ^{226}Ra , ^{210}Pb , and ^{228}Ra were retained very well.

418 Both for ^{232}Th and ^{40}K , a decrease in activity concentration was observed due to leaching and their
 419 release was influenced by the use of different alkali activators. The use of a sodium silicate solution

420 gave rise to the highest ^{232}Th leaching ($19.9 \pm 2.0\%$), while the use of sodium hydroxide solutions

421 resulted in the highest ^{40}K release ($75.8 \pm 14.1\%$ and $70.5 \pm 11.9\%$). Also the leaching of non-

422 radiological elements was affected by the use of different alkali activators. In general, only a small

423 amount of Al (0.5-0.8%), Ca (0.1-0.2%) and Si (0.1-0.3%) was mobilized, while the highest release was

424 observed for K (56-94%), Na (49-88%) and S (71-87%). ^{40}K showed the same leaching behavior as K

425 and Na, while for ^{232}Th it was concluded that the formation of multiple leachable thorium complexes

426 was responsible for its release. The extent to which these complexes individually contribute to

427 leaching, and the influence of the alkali activator on their formation, forms a subject of further study.

428 At first glance, drinking water is not endangered by leaching of NOR following the requirements of

429 the European Drinking Water Directive. The non-radiological elements of concern in this regard are

430 Al, Cl, F, Na and S, for which modelling and monitoring is required in case these AAMs are used in the
431 immediate vicinity of a drinking water supply. Also the pH should be monitored, since its value
432 should not exceed 9.5 for drinking water purposes. From the MIP results, it was concluded that both
433 the porosity and formation of multiple leachable and non-leachable complexes are determining
434 factors for the release of elements from AAMs.

435

436 **Acknowledgements**

437 This work was supported by the fund for scientific research Flanders (FWO), and hosted by the
438 University of Hasselt, the KU Leuven and the University of Texas. The authors would like to thank
439 Jenny Put for the IC measurements and to acknowledge the networking support of the COST Action
440 TU1301, www.norm4building.org.

441

442 **References**

- 443 Altmaier, B.M., Neck, V., Müller, R., Fanghänel, T., 2005. Solubility of $\text{ThO}_2 \cdot x\text{H}_2\text{O}(\text{am})$ in carbonate
444 solution and the formation of ternary Th(IV) hydroxide-carbonate complexes. *Radiochim. Acta*
445 93, 83–92. <https://doi.org/10.1524/ract.93.2.83.59420>
- 446 Altmaier, M., Neck, V., Denecke, M.A., Yin, R., Fanghänel, T., 2006. Solubility of $\text{ThO}_2 \cdot x\text{H}_2\text{O}(\text{am})$ and
447 the formation of ternary Th(IV) hydroxide-carbonate complexes in NaHCO_3 - Na_2CO_3 solutions
448 containing 0-4 M NaCl. *Radiochim. Acta* 94, 495–500. [https://doi.org/10.1524/ract.2006.94.9-](https://doi.org/10.1524/ract.2006.94.9-11.495)
449 11.495
- 450 ASTM International, 2017. ASTM C204-17. Standard test methods for fineness of hydraulic cement by
451 air-permeability apparatus.
- 452 Bureau voor Normalisatie (NBN), 2010. EN 196-6. Methods of testing cement - Part 6: Determination
453 of fineness.
- 454 Cappuyns, V., Swennen, R., 2008. The use of leaching tests to study the potential mobilization of
455 heavy metals from soils and sediments: A comparison. *Water, Air, Soil Pollut.* 191, 95–111.
456 <https://doi.org/10.1007/s11270-007-9609-4>
- 457 Central Pollution Control Board, 2012. Guidelines for management and handling of phosphogypsum
458 generated from phosphoric acid plants (Final Draft). Delhi.
- 459 Choppin, G.R., Liljenzin, J.-O., Rydberg, J., 2001. *Radiochemistry and nuclear chemistry*, 3rd ed.
460 Elsevier Science & Technology, Woburn.

- 461 Colàs, E., Grivé, M., Rojo, I., Duro, L., 2013. The effect of gluconate and EDTA on thorium solubility
462 under simulated cement porewater conditions. *J. Solution Chem.* 42, 1680–1690.
463 <https://doi.org/10.1007/s10953-013-0054-2>
- 464 Contreras, M., Gázquez, M.J., García-Díaz, I., Alguacil, F.J., López, F.A., Bolívar, J.P., 2013. Valorisation
465 of waste ilmenite mud in the manufacture of sulphur polymer cement. *J. Environ. Manage.* 128,
466 625–630. <https://doi.org/10.1016/j.jenvman.2013.06.015>
- 467 Contreras, M., Martín, M.I., Gázquez, M.J., Romero, M., Bolívar, J.P., 2014. Valorisation of ilmenite
468 mud waste in the manufacture of commercial ceramic. *Constr. Build. Mater.* 72, 31–40.
469 <https://doi.org/10.1016/j.conbuildmat.2014.08.091>
- 470 Cook, R.A., Hover, K.C., 1993. Mercury porosimetry of cement-based materials and associated
471 correction factors. *Constr. Build. Mater.* 7, 231–240. [https://doi.org/10.1016/0950-](https://doi.org/10.1016/0950-0618(93)90007-Y)
472 [0618\(93\)90007-Y](https://doi.org/10.1016/0950-0618(93)90007-Y)
- 473 Council of the European Union, 2014. Council directive 2013/59/EURATOM, European Basic Safety
474 Standards (BSS) for Protection against Ionising Radiation. *Off. J. Eur. Union L* 13/1.
- 475 Council of the European Union, 2013. European drinking water directive 2013/51/EURATOM, laying
476 down requirements for the protection of the health of the general public with regard to
477 radioactive substances in water intended for human consumption. *Off. J. Eur. Union L* 296/12.
- 478 Croymans, T., Leonardi, F., Trevisi, R., Nuccetelli, C., Schreurs, S., Schroeyers, W., 2017. Gamma
479 exposure from building materials - A dose model with expanded gamma lines from naturally
480 occurring radionuclides applicable in non-standard rooms. *Constr. Build. Mater.* 159, 768–778.
481 <https://doi.org/10.1016/j.conbuildmat.2017.10.051>
- 482 European Committee for Standardization, 2016. CEN/TS 16637-3. Construction products: Assessment
483 of release of dangerous substances - Part 3: Horizontal up-flow percolation test.
- 484 Evans, N.D.M., 2008. Binding mechanisms of radionuclides to cement. *Cem. Concr. Res.* 38, 543–553.
485 <https://doi.org/10.1016/j.cemconres.2007.11.004>
- 486 Felipe-sotelo, M., Hinchliff, J., Field, L.P., Milodowski, A.E., Preedy, O., Read, D., 2017. Retardation of
487 uranium and thorium by a cementitious backfill developed for radioactive waste disposal.
488 *Chemosphere* 179, 127–138. <https://doi.org/10.1016/j.chemosphere.2017.03.109>
- 489 Gijbels, K., Ion Iacobescu, R., Pontikes, Y., Vandevenne, N., Schreurs, S., Schroeyers, W., 2018. Radon
490 immobilization potential of alkali-activated materials containing ground granulated blast
491 furnace slag and phosphogypsum. *Constr. Build. Mater.* 184, 68–75.
492 <https://doi.org/10.1016/j.conbuildmat.2018.06.162>
- 493 Hjelmar, O., Wahlström, M., Comans, R., Kalbe, U., Grathwohl, P., Mehu, J., Schiopu, N., Hykš, J.,
494 Laine-ylijoki, J., van Zomeren, A., Krüger, O., Schoknecht, U., Wendel, T., Abdelghafour, M.,
495 Borho, N., 2012. Robustness validation of two harmonized European leaching tests for
496 assessment of the leaching of construction products, including waste-based construction
497 materials, in: WASCON 2012 Gothenburg, Sweden. pp. 1–5.
- 498 Huang, X., Zhuang, R., Muhammad, F., Yu, L., Shiao, Y., Li, D., 2017. Solidification/stabilization of
499 chromite ore processing residue using alkali-activated composite cementitious materials.
500 *Chemosphere* 168, 300–308. <https://doi.org/10.1016/j.chemosphere.2016.10.067>
- 501 International Atomic Energy Agency (IAEA), 2013. Radiation Protection and Management of NORM
502 Residues in the Phosphate Industry, Safety Reports Series No. 78. IAEA, Vienna.
503 <https://doi.org/10.1016/j.resourpol.2012.04.002>
- 504 Kitamura, A., Fujiwara, K., Mihara, M., Cowper, M., Kamei, G., 2013. Thorium and americium

505 solubilities in cement pore water containing superplasticiser compared with thermodynamic
506 calculations. *J. Radioanal. Nucl. Chem.* 298, 485–493. <https://doi.org/10.1007/s10967-013->
507 2618-4

508 Koplík, J., Kalina, L., Másilko, J., Šoukal, F., 2016. The characterization of fixation of Ba, Pb, and Cu in
509 alkali-activated fly ash/blast furnace slag matrix. *Materials (Basel)*. 9.
510 <https://doi.org/10.3390/ma9070533>

511 Kuo, W.-T., Wang, H.-Y., Shu, C.-Y., 2014. Engineering properties of cementless concrete produced
512 from GGBFS and recycled desulfurization slag. *Constr. Build. Mater.* 63, 189–196.
513 <https://doi.org/10.1016/j.conbuildmat.2014.04.017>

514 Lancellotti, I., Catauro, M., Dal, F., Kiventer, J., Leonelli, C., Illikainen, M., 2018. Alkali activation as
515 new option for gold mine tailings inertization. *J. Clean. Prod.* 187, 76–84.
516 <https://doi.org/10.1016/j.jclepro.2018.03.182>

517 Matzen, S.L., Beiriger, J.M., Torretto, P.C., Zhao, P., Viani, B.E., 2000. Uranium (VI) and neptunium (V)
518 transport through fractured, hydrothermally altered concrete. *Radiochim. Acta* 88, 657–664.
519 <https://doi.org/10.1524/ract.2000.88.9-11.657>

520 Michalik, B., de With, G., Schroeyers, W., 2018. Measurement of radioactivity in building materials -
521 Problems encountered caused by possible disequilibrium in natural decay series. *Constr. Build.*
522 *Mater.* 168, 995–1002. <https://doi.org/10.1016/j.conbuildmat.2018.02.044>

523 Mossini, E., Macerata, E., Giola, M., Mariani, M., 2015. Review of international normatives for natural
524 radioactivity determination in building materials. *Nukleonika* 60, 597–602.
525 <https://doi.org/10.1515/nuka-2015-0101>

526 Nebel, H., Spanka, G., 2013. Harmonisation of test methods for the execution of the european
527 construction products directive (CPD). Validation of a european leaching test for construction
528 products. *Waste and Biomass Valorization* 4, 759–767. <https://doi.org/10.1007/s12649-013->
529 9215-1

530 Nedeljković, M., Šavija, B., Zuo, Y., Lukovic, M., Ye, G., 2018. Effect of natural carbonation on the pore
531 structure and elastic modulus of the alkali-activated fly ash and slag pastes. *Constr. Build.*
532 *Mater.* 161, 687–704. <https://doi.org/10.1016/j.conbuildmat.2017.12.005>

533 Nguyen, H., Adesanya, E., Ohenoja, K., Kriskova, L., Pontikes, Y., Kinnunen, P., Illikainen, M., 2018. By-
534 product based ettringite binder - A synergy between ladle slag and gypsum. *Constr. Build.*
535 *Mater.* Submitted.

536 Nuccetelli, C., Pontikes, Y., Leonardi, F., Trevisi, R., 2015. New perspectives and issues arising from
537 the introduction of (NORM) residues in building materials: A critical assessment on the
538 radiological behaviour. *Constr. Build. Mater.* 82, 323–331.
539 <https://doi.org/10.1016/j.conbuildmat.2015.01.069>

540 Park, J.W., Hong, S.I., Yang, H.J., Lima, T., Ann, K.Y., 2014. Cement-free mortar using ground
541 granulated blast-furnace slag with different alkali-activators. *Appl. Mech. Mater.* 578–579,
542 1430–1440. <https://doi.org/10.4028/www.scientific.net/AMM.578-579.1430>

543 Provis, J.L., 2017. Alkali-activated materials. *Cem. Concr. Res.* (In Press).
544 <https://doi.org/10.1016/j.cemconres.2017.02.009>

545 Rand, M.H., Mompean, F.J., Perrone, J., Illemassène, M., 2008. Chemical thermodynamics of thorium.
546 OECD Pub.

547 Rashad, A.M., 2017. Phosphogypsum as a construction material. *J. Clean. Prod.* 166, 732–743.
548 <https://doi.org/10.1016/j.jclepro.2017.08.049>

549 Sas, Z., Doherty, R., Kovacs, T., Soutsos, M., Sha, W., Schroevers, W., 2017. Radiological evaluation of
550 by-products used in construction and alternative applications; Part I. Preparation of a natural
551 radioactivity database. *Constr. Build. Mater.* 150, 227–237.
552 <https://doi.org/10.1016/j.conbuildmat.2017.05.167>

553 Shakhshiro, A., Sansone, U., Wershofen, H., Bollhöfer, A., Kim, C.K., Kim, C.S., Kis-Benedek, G.,
554 Korun, M., Moune, M., Lee, S.H., Tarjan, S., Al-Masri, M.S., 2011. The new IAEA reference
555 material: IAEA-434 technologically enhanced naturally occurring radioactive materials
556 (TENORM) in phosphogypsum. *Appl. Radiat. Isot.* 69, 231–236.
557 <https://doi.org/10.1016/j.apradiso.2010.09.002>

558 Shi, C., Fernández-Jiménez, A., 2006. Stabilization/solidification of hazardous and radioactive wastes
559 with alkali-activated cements. *J. Hazard. Mater.* 137, 1656–1663.
560 <https://doi.org/10.1016/j.jhazmat.2006.05.008>

561 Sutton, M., Warwick, P., Hall, A., 2003. Uranium (VI) interactions with OPC/PFA grout. *J. Environ.*
562 *Monit.* 5, 922. <https://doi.org/10.1039/b308554f>

563 Sylwester, E.R., Hudson, E.A., Allen, P.G., 2000. The structure of uranium (VI) sorption complexes on
564 silica, alumina, and montmorillonite. *Geochim. Cosmochim. Acta* 64, 2431–2438.
565 [https://doi.org/10.1016/S0016-7037\(00\)00376-8](https://doi.org/10.1016/S0016-7037(00)00376-8)

566 Tänzer, R., Jin, Y., Stephan, D., 2017. Alkali activated slag binder: effect of cations from silicate
567 activators. *Mater. Struct. Constr.* 50. <https://doi.org/10.1617/s11527-016-0961-y>

568 Tayibi, H., Choura, M., López, F.A., Alguacil, F.J., López-Delgado, A., 2009. Environmental impact and
569 management of phosphogypsum. *J. Environ. Manage.* 90, 2377–2386.
570 <https://doi.org/10.1016/j.jenvman.2009.03.007>

571 Tits, J., Walther, C., Stumpf, T., Macé, N., Wieland, E., 2015. A luminescence line-narrowing
572 spectroscopic study of the uranium (VI) interaction with cementitious materials and titanium
573 dioxide. *Dalt. Trans.* 44, 966–976. <https://doi.org/10.1039/c4dt02172j>

574 Ulubeyli, G.C., Artir, R., 2015. Sustainability for blast furnace slag: Use of some construction wastes.
575 *Procedia - Soc. Behav. Sci.* 195, 2191–2198. <https://doi.org/10.1016/J.SBSPRO.2015.06.297>

576 Wang, L., Yu, K., Li, J., Tsang, D.C.W., Poon, C.S., Yoo, J., Baek, K., Ding, S., Hou, D., Dai, J., 2018. Low-
577 carbon and low-alkalinity stabilization/solidification of high-Pb contaminated soil. *Chem. Eng. J.*
578 351, 418–427. <https://doi.org/10.1016/j.cej.2018.06.118>

579 Washburn, E.W., 1921. Note on a method of determining the distribution of pore sizes in a porous
580 material. *Proc. Natl. Acad. Sci.* 7, 115–116.

581 Wellman, D.M., Mattigod, S. V., Arey, B.W., Wood, M.I., Forrester, S.W., 2007. Experimental
582 limitations regarding the formation and characterization of uranium-mineral phases in concrete
583 waste forms. *Cem. Concr. Res.* 37, 151–160. <https://doi.org/10.1016/j.cemconres.2006.11.004>

584